AIP | Physics of Plasmas

Magnetohydrodynamic modes analysis and control of Fusion Advanced Studies Torus high-current scenarios

F. Villone, G. Calabrò, G. Marchiori, S. Mastrostefano, G. Vlad, T. Bolzonella, F. Crisanti, V. Fusco, Y. Q. Liu, P. Mantica, L. Marrelli, and P. Martin

Citation: Physics of Plasmas (1994-present) **21**, 082514 (2014); doi: 10.1063/1.4893418
View online: http://dx.doi.org/10.1063/1.4893418
View Table of Contents: http://scitation.aip.org/content/aip/journal/pop/21/8?ver=pdfcov
Published by the AIP Publishing

Magnetohydrodynamic modes analysis and control of Fusion Advanced Studies Torus high-current scenarios

F. Villone,[1] G. Calabrò,[2] G. Marchiori,[3] S. Mastrostefano,[1] G. Vlad,[2] T. Bolzonella,[3] F. Crisanti,[2] V. Fusco,[2] Y. Q. Liu,[4] P. Mantica,[5] L. Marrelli,[3] and P. Martin[3]
[1]*Euratom-ENEA-CREATE Ass., DIEI, Univ. di Cassino e Lazio Merid., Cassino (FR), Italy*
[2]*C. R. Frascati, Euratom-ENEA Ass., Via E. Fermi 45, 00044 Frascati, Italy*
[3]*Cons. RFX, Euratom-ENEA-RFX Ass., Corso Stati Uniti 4, 35127 Padova, Italy*
[4]*Euratom/CCFE Fusion Association, Culham Science Centre, Abingdon OX14 3DB, United Kingdom*
[5]*IFP-CNR, Euratom-ENEA-CNR Ass. Via Cozzi 53, 20125 Milano, Italy*

(Received 6 May 2014; accepted 5 August 2014; published online 20 August 2014)

One of the main FAST (Fusion Advanced Studies Torus) goals is to have a flexible experiment capable to test tools and scenarios for safe and reliable tokamak operation, in order to support ITER and help the final DEMO design. In particular, in this paper, we focus on operation close to a possible border of stability related to low-q operation. To this purpose, a new FAST scenario has then been designed at $I_p = 10$ MA, $B_T = 8.5$ T, $q_{95} \approx 2.3$. Transport simulations, carried out by using the code JETTO and the first principle transport model GLF23, indicate that, under these conditions, FAST could achieve an equivalent $Q \approx 3.5$. FAST will be equipped with a set of internal active coils for feedback control, which will produce magnetic perturbation with toroidal number $n = 1$ or $n = 2$. Magnetohydrodynamic (MHD) mode analysis and feedback control simulations performed with the codes MARS, MARS-F, CarMa (both assuming the presence of a perfect conductive wall and using the exact 3D resistive wall structure) show the possibility of the FAST conductive structures to stabilize $n = 1$ ideal modes. This leaves therefore room for active mitigation of the resistive mode (down to a characteristic time of 1 ms) for safety purposes, i.e., to avoid dangerous MHD-driven plasma disruption, when working close to the machine limits and magnetic and kinetic energy density not far from reactor values. © *2014 AIP Publishing LLC*.
[http://dx.doi.org/10.1063/1.4893418]

I. INTRODUCTION

An ITER accompanying program, in view of DEMO, is presently under development, with different collaborations, between the ITER partners. The Advanced Scenarios dedicated satellite, JT60-SA,[1] is under construction in Japan, in order to fully investigate the actual possibility to design a steady state DEMO, with enhanced energy confinement properties. A current matter of concern is a possible optimal experiment to support ITER operations problems (giant Edge Localized Modes (ELMs), disruptions, plasma controls, etc.) and to tackle the challenging problem of the power exhaust in view of DEMO. In this stream, the FAST (Fusion Advanced Studies Torus) device (major radius $R = 1.82$ m, minor radius $a = 0.64$ m, plasma current $I_p = 8$ MA, toroidal field $B_T = 8.5$ T) is presently under discussion as a possible DEMO and ITER satellite.[2] The main FAST goals are, in order of priority, exploring plasma wall interaction (with particular attention to the power exhaust problem[3]) in reactor relevant conditions; testing tools and scenarios for safe and reliable tokamak operation up to the border of stability, with particular attention on avoiding disruptions; studying fusion plasmas with a significant population of fast particles. Since the main FAST target is the study of the integrated, bulk plasma and divertor region, power exhaust problem, a strong effort has been put on the design of the First Wall (FW) and of the divertor (in Tungsten and capable to sustain up to 20 MW/m^2). A Tungsten coated FW is envisaged, capable to sustain up to a peak power around 5 MW/m^2.[4] The poloidal circuit has the capacity to produce a Snow Flake (SF) configuration, for the reference scenario, with a reduction of the plates power flux larger than a factor 5.[5] A new divertor has been designed with the possibility, within the same discharge, to switch from a standard X point to a SF one.[6] One of the FAST peculiarities is the capability of addressing all of these items simultaneously in a single, fully integrated scenario with dimensionless physics parameters close to DEMO and ITER. In this sense, FAST is fully complementary to JT60-SA, whose main target is to study and to optimize the advanced regimes, in view of DEMO.

The present paper aims at studying an upgrade of the FAST reference scenario, focusing on low-q operation, which allows exploring 10 MA plasmas. In particular, we refer to regions with $2 < q_{95} < 2.7$ (here q_{95} is the value of the safety factor at the flux surface which includes the 95% of the poloidal flux) that are interesting to push fusion performances, but could be too risky to be tested in ITER. The main goal of this paper, of course, is not to show the possibility of increasing the machine performances, neither to perform an exhaustive description of the proposed scenarios. Rather, the actual main goal is to show the possibility to achieve a very high magnetic and kinetic energy density scenario, at very low q_{95}, and to describe the development of some safe and robust control tools to possibly mitigate the occurrence of magnetohydrodynamic (MHD) driven

disruptions, related to operation close to this specific stability limit. Specifically, we investigate a new FAST scenario at $I_p = 10$ MA, $B_T = 8.5$ T, with a $q_{95} \approx 2.3$ that would correspond to $I_p \approx 20$ MA in ITER. The possibility to safely work at $q_{95} < 3$ ($q_{95} \approx 2.6$) has been shown recently at JET,[7] although with a slight degradation of the energy confinement ($H_{98} \approx 0.9$). The key point is to demonstrate in FAST, for such a low-q scenario, the possibility of using passive conducting structures and active coils to stabilize and control potentially dangerous ideal and resistive MHD modes. To this purpose, FAST will be equipped with a set of feedback controlled active coils[8] located between the first wall and the vacuum vessel and accessible for maintenance with the remote handling system, carrying currents up to 20 kA with AC frequency up to few kHz. The final target of such a MHD feedback loop is not necessarily the full stabilization of plasma operation at this very low q_{95} values, but at least the availability of a feedback control system able to mitigate the effects of potentially disruptive MHD activity, after detection of its onset. If successful, this would give the opportunity to change the operational point, so as to avoid the disruption and, possibly, even a controlled plasma shut down, in order to rebuild the plasma reference conditions, in a time as short as possible.

The paper is organized as follows. Section II reports some details about scenario development and related transport analysis. Section III is dedicated to MHD modes analysis, both for ideal and resistive plasma, in the presence of conducting structures with increasing level of geometrical details. Section IV illustrates the capabilities of the in-vessel active coils to effectively feedback control some of the unstable MHD modes, under different assumptions on the controller architecture. Finally, Sec. V draws the conclusions.

II. DEVELOPMENT OF 10 MA SCENARIOS

A. Equilibrium configurations

It is well known that, lowering the edge safety factor, both the kink and the tearing MHD modes become more unstable,[9] hence setting an upper limit to the plasma current (at fixed size and toroidal field) in order to avoid hard disruptions. However, following a suitable trajectory in the q_{95}-l_i plane during the plasma current ramp-up, it is possible to reach plasma equilibria at the very low $q_{95} \geq 2$.[9] This can be even easier in X-point tokamak configurations, thanks to the stabilizing role played by the strong edge magnetic shear. Recent JET experiments,[7] with $q_{95} \approx 2.6$, have confirmed the possibility to safely work at $q_{95} < 3$ even for large machines at very high plasma current. Moreover, other experiments (performed on RFX operated as a Tokamak[10] and recently confirmed by some very preliminary tests on DIII-D[11,12]) have hinted at the possibility of using active coils to control the Resistive Wall Mode (RWM) when operating at $q_{95} \approx 2$. These facts have encouraged to study the possibility of FAST scenarios up to $q_{95} \geq 2$.[13] In particular, several different equilibria have been studied to check the possibility to have a class of plasmas with a slightly different current profile, hence with different stability properties.

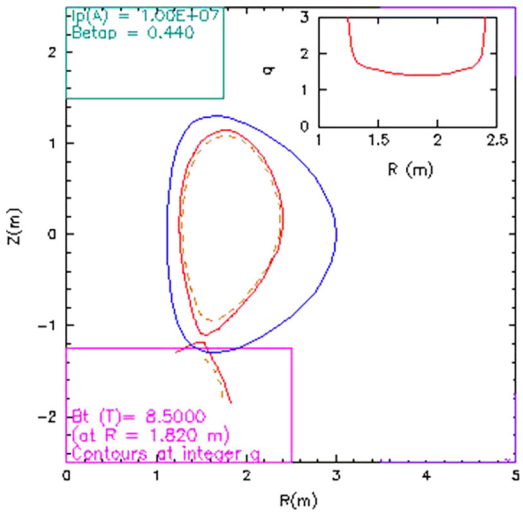

FIG. 1. Iso-q(ψ) map; q95 and q(ψ) = 2 surfaces are shown. The blue line is a simplified representation of the conducting structures. In the inset, the q_ψ(R) profile is reported.

The main guideline for the development of the new configurations is not to achieve an exhaustive scan of the $q_{95} - l_i$ plane, but rather to get equilibria with both a low q_{95} and a low l_i. This describes a potential experimental situation where it is possible to achieve the low q_{95} regime yet retaining stability as much as possible. For all the equilibria, the plasma current is $I_p = 10$MA and the poloidal beta $\beta_p = 0.44$. The minor plasma radius slightly changes, allowing a variation of q_{95}. The current density profiles are varied to get different pairs of q_{95}-l_i values. In Fig. 1, we show the typical q(ψ) map and the q(R) profile. The closeness of the q(ψ) = 2 surface to the plasma boundary suggests a possible interaction of the modes associated with this surface with the FAST conductive structures, and the possibility to stabilize these modes by active coils. The absence of the q(ψ) = 1 surface is an artefact introduced to allow linear MHD codes to easily study the tearing and external kink instabilities.

Four different equilibria have been produced, which are described in Table I.

The MHD analysis reported in the following sections shows substantially different stability properties for these equilibria. These differences are largely due to different q profiles, as shown in Fig. 2. Of course, an accurate tailoring of the current rise[7] and of the plasma heating will be necessary to drive the current profile towards the most convenient (stable) situation. An internal q = 1 surface may eventually appear; nevertheless, in the present study, we have considered only equilibria without a q = 1 surface, in order to allow an easier analysis of external kink and tearing instabilities. This could lead to the development of sawteeth; if these are

TABLE I. Parameters of the equilibrium configurations analyzed.

Equilibrium	$q_{boundary}$	q_{axis}	q_{95}	l_i	a (m)	β_N
EQ#1	2.62	1.58	1.94	0.46	0.589	1.944
EQ#2	2.61	1.68	2.06	0.47	0.622	1.915
EQ#3	2.75	1.40	2.02	0.57	0.646	1.934
EQ#4	2.92	1.29	1.95	0.63	0.644	1.943

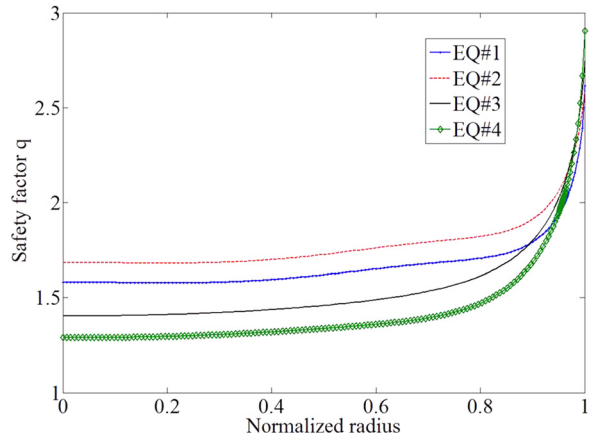

FIG. 2. Safety factor profiles for various equilibria.

sufficiently small, the plasma discharge may not be significantly affected.[7]

It is worth noticing that no details of the pedestal (described in the following section) and of the associated bootstrap currents have been considered in the equilibrium configurations. Indeed, we will demonstrate in the following that the introduction of such details would give rise to rather insignificant changes in the stability properties. Such modifications can be considered as perturbations for the MHD analysis and the feedback control of instabilities, reported in the following sections.

B. Transport analysis

In order to estimate the kinetic profiles (n_e, T_i, T_e) and confinement time that can be expected in the 10 MA/8.5 T FAST scenario, predictive transport simulations have been performed using the JETTO 1.5D transport solver[14] with one of the equilibria described earlier, but evolving the current density profile using neoclassical resistivity. The GLF23 model[15] has been used to predict the n_e, T_i, and T_e profiles, but effects of rotation have been neglected, since as discussed in Ref. 16 they are generally small in H-mode plasmas and become significant only in Advanced Tokamak scenarios. The heating applied was 30 MW of ICRH in (^{3}He)-D minority, of which ~20 MW deposited collisionally to thermal ions and 7.5 MW to electrons, mostly collisionally. Z_{eff} was set to 1.5 and radiated power was 5 MW. Pedestal values of n_e ($3.2 \times 10^{20}\,m^{-3}$) and T_i, T_e (4 keV) have been chosen in order for the total confinement to follow the standard H-mode confinement scaling law, with $H_{98} \sim 0.82$ taking into account the observation of confinement reduction in JET scenarios at low q_{95}. We notice that the transport simulations presented here concern only the core transport. No attempt has been made to simulate by first principles or empirical models the complex physics of the pedestal in FAST, for which there is ongoing separate work[16] outside the scope of the present paper. Instead, a boundary condition has been assumed for density and temperature at the top of the pedestal, which has been estimated with a simplified procedure. We know from Refs. 13 and 14 that in H-mode plasmas, the pedestal energy is proportional to the total plasma energy as $W_{ped} \sim 40\%\ W_{tot}$. From these considerations, together with the value of the H factor (which is seen ~0.8 in low q_{95} JET H-modes), we can calculate the temperature at pedestal top, knowing the mean plasma density value. This last quantity has been assumed at about 50% of the Greenwald limit.[15] There would still be margin for higher densities which would result in lower pedestal temperatures. However, the case presented here has been chosen as an example of the type of profiles that can be expected.

The steady-state profiles obtained are shown in Fig. 3. The total energy confinement time was 0.5 s and the equivalent fusion gain $Q_{DT} = 3.7$.

III. MHD ANALYSIS

A. Ideal modes

We focus on $n = 1$ ideal modes, computing the ideal-wall limit position with the MARS[17] and MARS-F[18] codes for the equilibria described above. A sensitivity analysis on the safety factor q at plasma boundary (keeping the q profile substantially unchanged) shows that for the above equilibria the $n = 2$ current-driven ideal kink is stable, and hence this mode will not be further analysed in the present paper. However, high-beta operation might possibly destabilize the pressure driven $n = 2$ ideal kink, and so a deeper analysis might be necessary in this case. This will be addressed in future activity.

Fig. 4 shows the instability growth rate γ (normalized to the on-axis Alfvén time τ_A) as a function of the position b of an ideal wall, conformal to the boundary of the plasma, whose minor radius is a. For EQ#1, the ideal wall limit position is around $1.32a$, while for EQ#2 it is around $1.25a$ and for EQ#3 it is around $1.41a$. Conversely, for EQ#4, the $n = 1$ ideal kink is stable for any position of the conducting wall (even with wall at infinity). These differences are due to the different q profiles which characterize the considered equilibria, as shown in previous section. In order to investigate this property of EQ#4, we have carried out a thorough sensitivity analysis, scanning both the boundary value of q (done for all the equilibria, as reported above) and, in addition, also

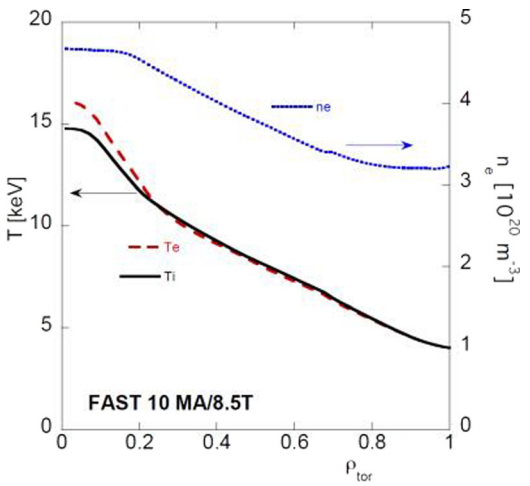

FIG. 3. Steady-state profiles of n_e, T_i, T_e simulated for the FAST 10 MA/8.5 T scenario using the GLF23 model in the JETTO transport code.

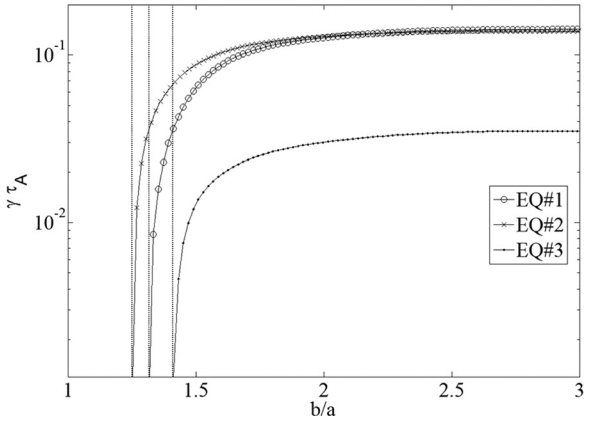

FIG. 4. Growth rate behaviour and ideal wall limiting positions (dashed vertical lines).

the plasma pressure. This analysis has confirmed that the $n=1$ current-driven ideal kink is stable for EQ#4. Similar results apply to the $n=2$ current-driven ideal kink.

The sensitivity analysis on the boundary value of q allows us to evaluate the effect on $n=1$ ideal kink stability of the approximation of the plasma boundary, which is required by the fact that the configurations under analysis correspond to diverted equilibria with an X-point, which cannot be treated by MARS and MARS-F. In particular, for EQ#3, a thorough scan of the boundary value of q shows that the no-wall growth rate can exceed the nominal value (reported in Fig. 4) only by around 10%.

A dedicated analysis has been carried out to test the importance of the introduction of pedestal details into the equilibrium configuration. A strong pedestal may introduce a significant boostrap current density, peaked towards the edge of the plasma. This may have a localized effect on the edge q profile; however, the expected effect is small, since low-*n* external kink instability (which is the focus of the present analysis) may not be significantly affected by such localized changes. Conversely, the modifications of the q profile close to the edge can be of primary importance for other MHD modes such as the peeling mode or the edge localized infernal mode, which are not addressed in this paper.

We considered the profiles reported in Fig. 5, which correspond to the introduction in EQ#3 of a pedestal structure similar to what was discussed in previous section. Repeating the above analysis, we found a rather insignificant change of the ideal wall limit position (less than 4%) and of the mode structure. This demonstrates that this aspect can be considered as a small perturbation of the analysis reported in the present section and of the feedback control of instabilities, reported in the following.

Focusing the attention on the first three equilibria, for which the $n=1$ external kink is potentially unstable, it is important to investigate the effect of the actual conducting structures of FAST (vessel, conducting plates, active coils). If such conducting structures are close enough to the plasma (i.e., inside the limiting position for complete stabilization, as shown in Fig. 4), they could in principle stabilize the mode if they were made of an ideal conductor, thanks to eddy currents induced by plasma perturbations. Due to the

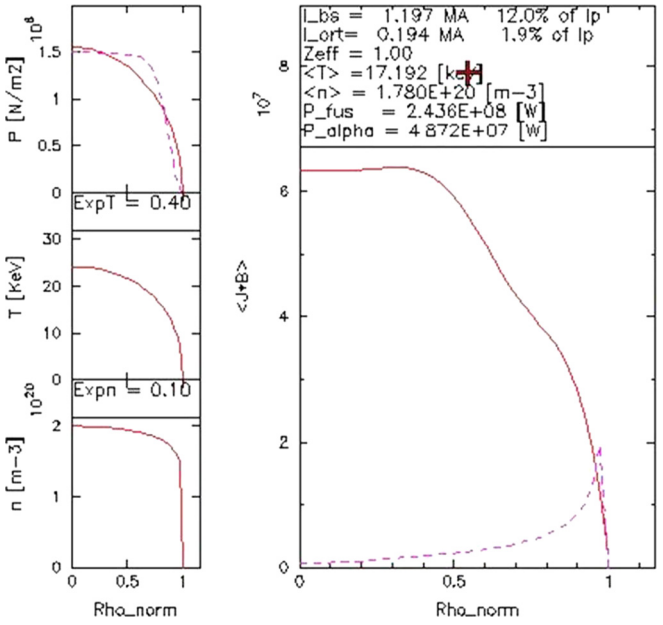

FIG. 5. Effect of pedestal and associated bootstrap current density (dashed).

finite resistivity of such conductors, these eddy currents will eventually decay, allowing instabilities to grow, with a "slow" electromagnetic time constant rather than the "fast" Alfvén time scale. In these conditions, a RWM can develop, and it can be, possibly, actively controlled magnetically with suitable feedback coils.

Since the geometry of the conducting structures in FAST is rather complex and quite far from being conformal to the plasma as assumed by 2D equilibrium codes (as the ones used by MARS and MARS-F), the CarMa computational tool[19,20] has been applied, allowing a realistic fully three-dimensional treatment of such conductors. In particular, a 3D finite element mesh of the vacuum vessel has been produced, in which the port extensions have been simulated with some conducting patches with a resistivity somewhat higher than the bulk value of 1.29 $\mu\Omega$m. No conducting plates have been introduced, since it has been demonstrated[21] that their poloidal coverage is too narrow to have a significant effect on external kink stabilization. Several electromagnetic modes and the corresponding time constants have been computed, also making a Fourier analysis of the dominant toroidal and poloidal harmonics (*n*,*m*) (Fig. 6 and Table II). We notice that the values reported in Table II are purely electromagnetic time constants of the conducting structures. Moreover, the same (*n*,*m*) dominant harmonic may be present in different electromagnetic modes (e.g., an axisymmetric current flowing either in the toroidal or in the poloidal direction).

Coupling this model of the conducting structures with the plasma responses corresponding to the aforementioned equilibria, we found that for EQ#1 and EQ#2 the instability growth rate is still on the Alfvén time scale, hence making any magnetic active control practically unachievable. Note that, in this analysis, we are neglecting the possible stabilizing contribution of plasma flow and kinetic damping. Conversely, for EQ#3 a true RWM is present; its growth rate is of the order of $450\,s^{-1}$ when neglecting the port

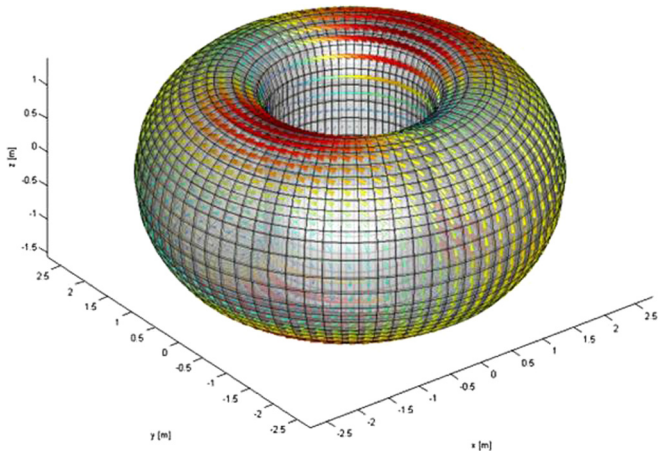

FIG. 6. Finite elements mesh and current density pattern corresponding to the slowest n = 1, m = 1 mode.

extensions. In this case, an active magnetic control of the instability might be feasible, as discussed in next section.

B. Resistive modes

Low-q configurations are particularly prone to non-ideal modes, e.g., tearing modes.[22] Hence, a non-ideal mode analysis has been carried out, using MARS and MARS-F codes, on the low-q FAST configurations under analysis in this paper, specifically on EQ#3 reported above.

The analysis has considered plasma resistivity η such that the corresponding Lundquist number S ranges from $S = 10^6$ to $S = 10^9$, the Lundquist number being defined as the ratio between the resistive and Alfvén time, $S \equiv (4\pi a^2 v_A/\eta c^2 R_0)$ (here, v_A is the Alfvén velocity). Typical expected values for FAST plasmas are in the range $S \approx 10^8$–10^9.

First of all, we computed the $n = 1$ mode growth rate γ and mode frequency ω for various positions of an axisymmetric conformal wall varying the wall minor radius b. Figure 7 shows the growth rate γ (normalized to the on-axis Alfvén time), for various values of plasma resistivity; both the ideal wall case and the resistive wall case are reported.

For typical values of plasma resistivity, and for wall positions significantly inside the limiting position for ideal mode stabilization, the growth rate is considerably slower than Alfvénic time scale. Moreover, the nature of the mode drastically changes, as the wall minor radius is decreased below the limiting position, transforming from a spatially diffused perturbation (with a dominant $m = 3$ poloidal component) to a highly localized one around the $q = 2$ surface (hence, with a dominant $m = 2$ poloidal component), as it can be seen in Fig. 8 (ideally conducting wall, $b/a = 1.2$, $S = 10^8$).

TABLE II. A few vessel electromagnetic time constants (ms).

η_{patch}	1.29 $\mu\Omega$m	2.5 $\mu\Omega$m	5 $\mu\Omega$m
Mode			
$n = 0, m = 0$ (toroidal)	34.6	27.3	21.8
$n = 0, m = 0$ (poloidal)	14.3	13.4	12.7
$n = 0, m = 1$ (up-down antisymmetric)	17.9	15.0	13.1
$n = 1, m = 1$ (up-down)	24.2	20.3	17.8
$n = 1, m = 1$ (inboard-outboard)	15.3	12.4	10.1

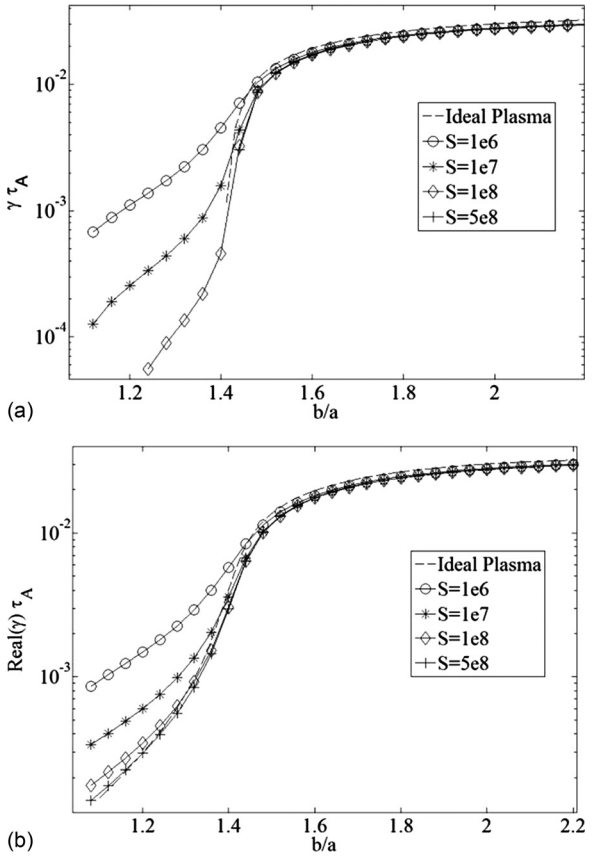

FIG. 7. Non-ideal mode growth rate (normalized to on-axis Alfvén time), as a function of the wall minor radius, (normalized to the plasma minor radius a) for various values of plasma resistivity: (a) ideal wall and (b) resistive wall.

Considering an ideal wall located at $b/a = 1.12$, we made a scan of the plasma resistivity. The growth-rate scales approximately as $\gamma \propto S^{-3/5}$ for $10^6 \le S \le 1 \times 10^7$ (thus

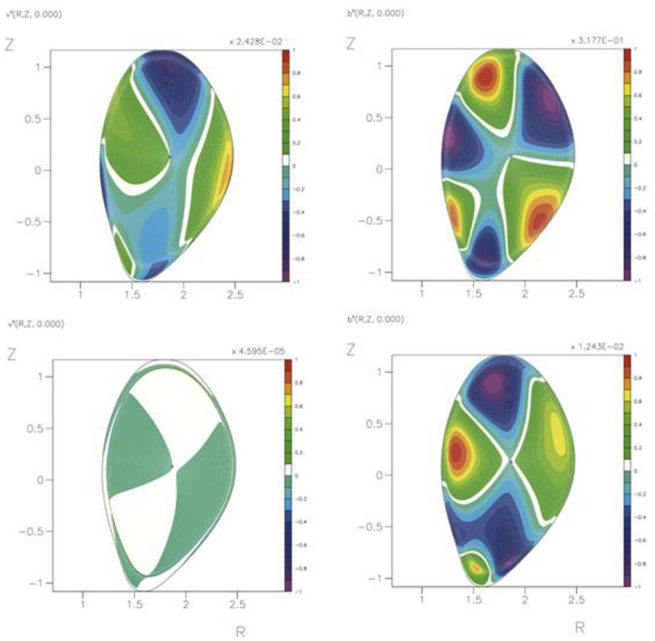

FIG. 8. Unstable mode structure inside the plasma: radial components of perturbed velocity (left) and magnetic field (right) for an ideal (top, $b/a = 1.6$) and a resistive mode (bottom, $b/a = 1.2$, $S = 10^8$).

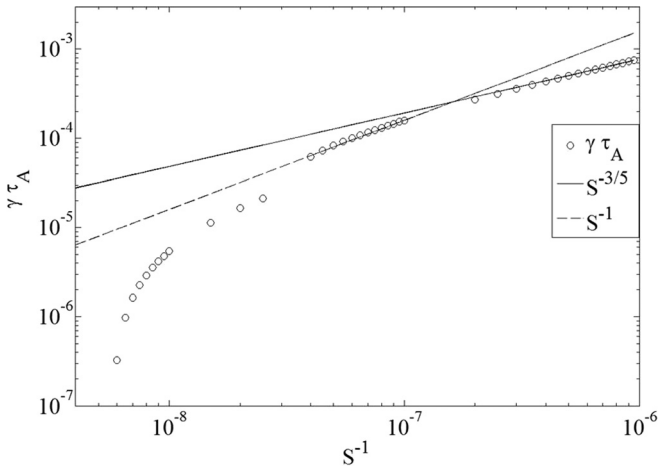

FIG. 9. Growth-rate γ vs. the inverse of the Lundquist number S^{-1} for $b/a = 1.12$.

showing the tearing nature of the mode) and almost linearly with the inverse of the Lundquist number, $\gamma \propto S^{-1}$, for higher values, $S > 10^7$ (Fig. 9).

In Fig. 10, the eigenvalues, as result from the scan of the plasma resistivity, are shown in the plane (γ, ω). For Lundquist numbers above a certain threshold (about 3×10^7), two modes appear, corresponding to complex conjugate eigenvalues. This is to be theoretically expected for tearing modes.

IV. ACTIVE FEEDBACK CONTROL OF MHD MODES IN FAST

The active feedback control of MHD modes, and specifically of RWMs, has received increasing attention in recent years. The comprehensive review paper[23] illustrates clearly the recent advances and the present state of the art, for both magnetic and rotational stabilization of RWMs. In particular, several devices have shown experimentally significant advances in the feedback active stabilization of RWMs, like for instance DIII-D[24,25] and NSTX.[26] In addition, many numerical stability and control analyses have been dedicated to ITER,[27,28] resorting to available 3D RWM codes like CarMa (used in the present paper) or others.

The goal of this final section of the present paper is not to develop new techniques for the feedback control of RWM,

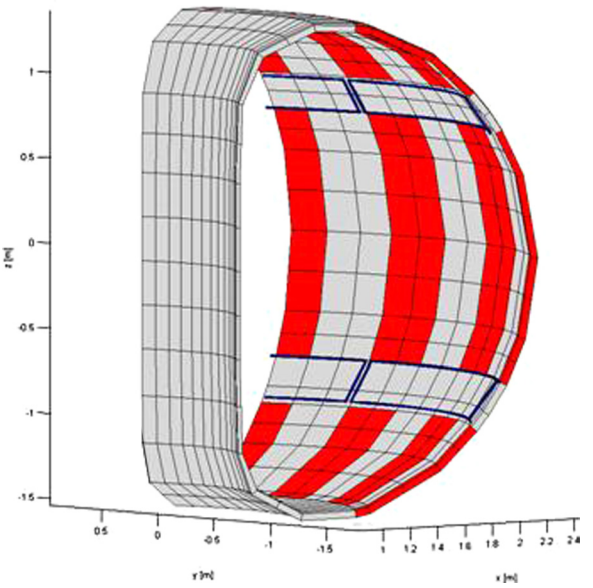

FIG. 11. Cutaway view of the three-dimensional finite elements mesh of vessel (gray), ports (red), active coils (blue). The actual mesh spans 360° in the toroidal direction.

but rather to demonstrate that low-q FAST configurations described previously can be successfully feedback controlled with the available in-vessel coils, and to quantify the expected requirements on power supplies. To this purpose, a model-based approach is used, which relies on the development of a complete simulator, including a model of the plasma, the active conductors, the passive structures, the diagnostics, the feedback controller, and the signal processing blocks. The same model-based approach has been successfully applied and experimentally validated on RFX-mod[29] and can be used for other future devices, in addition to FAST.

A. Architecture of the feedback system

In this section, we investigate the possibility of feedback controlling the unstable $n = 1$ RWM described in the previous section with reference to EQ#3. To this purpose, the computational model has been enhanced with a set of 18 active feedback coils,[8] whose mesh is reported in Fig. 11. The coils are subdivided in two arrays of 9 coils aligned along the torus: the first one in the gap between the upper and equatorial port, the second one in the gap between the

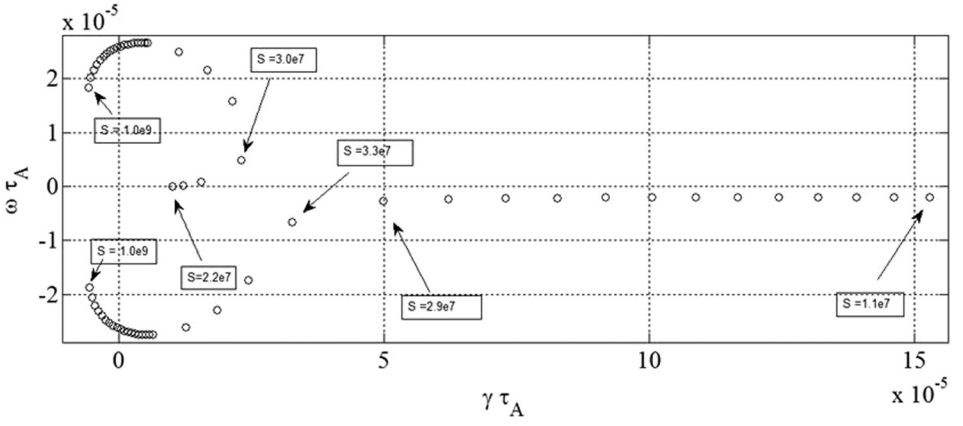

FIG. 10. Mode growth rate γ and frequency ω, for various values of Lundquist number S.

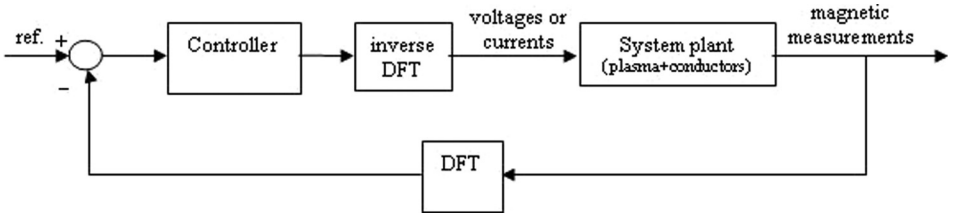

FIG. 12. Block diagram of feedback system.

equatorial port and the lower port. Each coil is considered as single-turn, with a resistance of 6 $\mu\Omega$.

The simulated magnetic field measurements at various points are assumed as output. In particular, three locations in the poloidal plane have been selected (midplane; below the upper coils; below the lower coils). For each poloidal location, a fictitiously high number of measurement points are considered at several toroidal angles, in order to neglect aliasing problems.

A discrete Fourier transform (DFT) is applied on the simulated measurements to get the $n=1$ feedback signal, which is processed by the controller providing a reference $n=1$ distribution of current or voltage for the active coils. Due to the difference between the number of sensors and coils, this $n=1$ current or voltage distribution is then resampled along the toroidal coordinate according to the coil periodicity and a reference signal for each upper and lower coil can be obtained. Fig. 12 shows the block diagram of the feedback control.

An eigenvalue analysis of the open loop plasma response has been carried out; unstable modes and stable modes with time responses slower than 10 ms have been considered. The calculation yielded a couple of $n=1$ unstable modes (sine/cosine components) with a growth rate around 450 s^{-1}. The corresponding magnetic field components have been evaluated. The magnetic field tangential component in the poloidal plane at the midplane (Bt) and the normal component (Bn) under the upper and lower active coils are shown in Fig. 13 (central, upper, and lower plot, respectively). In general, the unstable mode can be represented as a linear combination of the two $n=1$ magnetic field distributions presented in the figure (red and blue curve in each plot). The inspection of the curves at different poloidal positions can provide some hints on the spatial structure of the unstable mode along the poloidal coordinate. In particular, a phase shift of about 180° between the normal component Bn at the uppermost and lowermost positions can be noticed, while the tangential component at midplane exhibits a phase

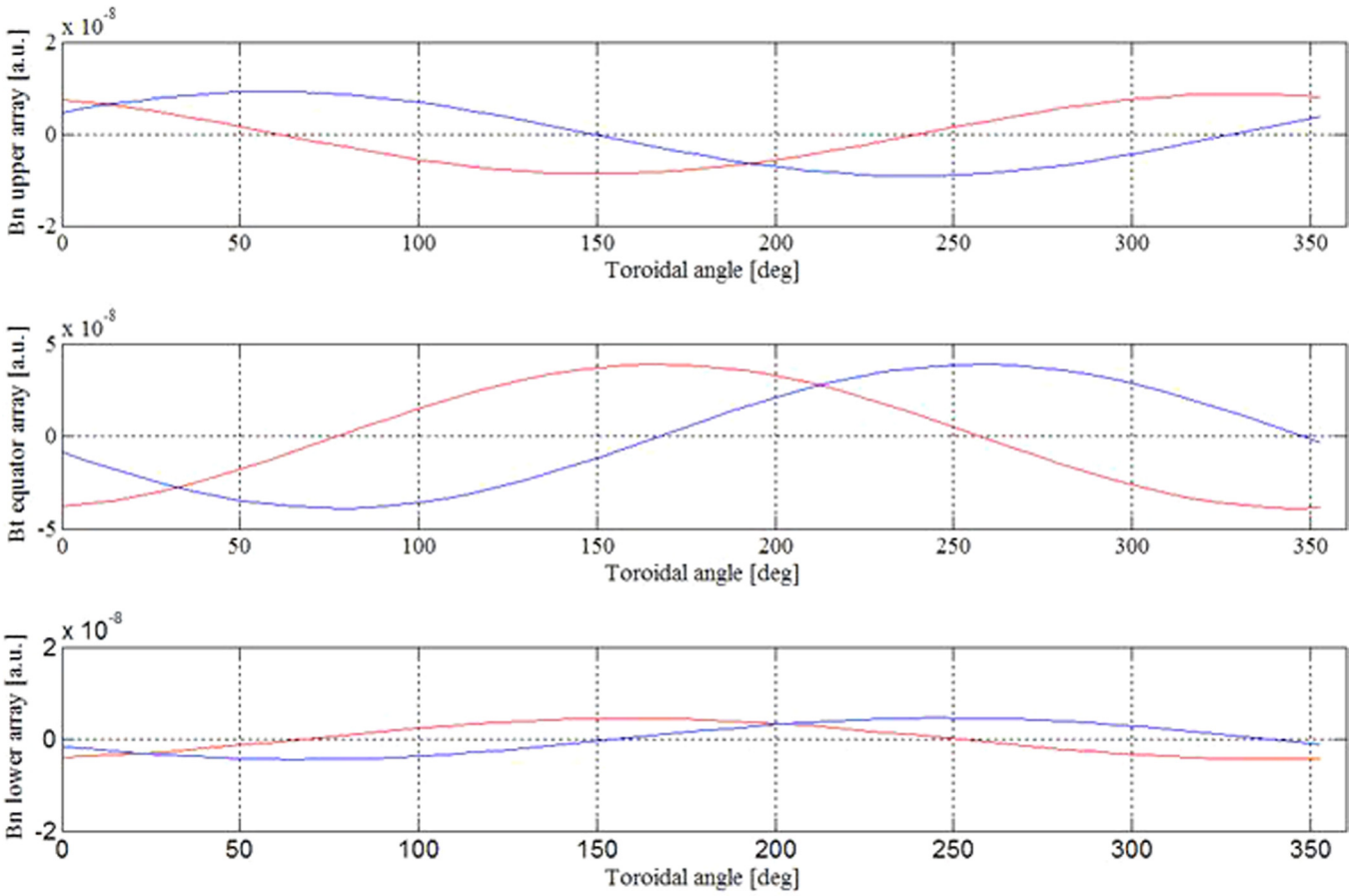

FIG. 13. Magnetic field normal (Bn) and tangential (Bt) components along the torus at different poloidal positions: the spatial patterns shown in the plots make up a base to represent the unstable $n=1$ mode.

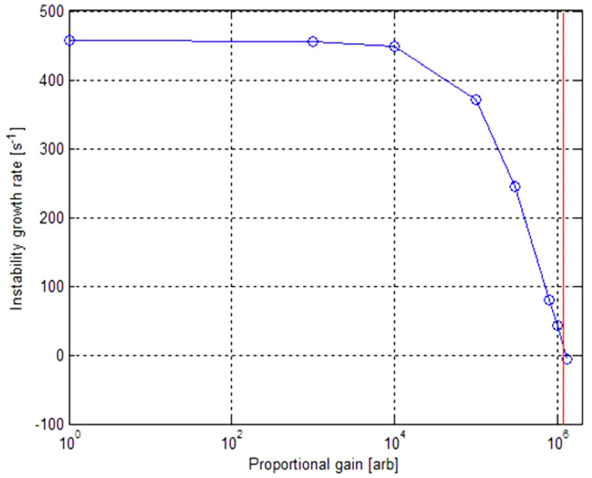

FIG. 14. Current-based proportional feedback controller (red vertical line: critical gain).

shift of about 90° with respect to the normal components under the active coils. These features of the plasma response were taken into account in the design of the feedback control system. Other stable modes with a dominant $n = 1$ content are present, with time constants ranging from 450 ms to 10 ms. The slowest of such $n = 1$ stable modes are associated with the low resistance, single turn configuration of the active coil adopted in this stage of the design.

B. Current-based feedback control

First of all, we consider a feedback controller acting on the $n = 1$ component of the current in the active coils.

Evidently, in a practical implementation, a dedicated current regulator would be needed in each coil; this is neglected in the present study, hence considering the current regulation as ideal.

On the basis of the results observed in different experimental devices,[30] the tangential component of the magnetic field was selected for the design of a first feedback control system of the unstable mode. Since the magnetic field produced by the coil system at the sensor position is mainly normal, this choice could be seen as a way to decouple the feedback signal from the effect of the actuators themselves. Nonetheless, we also considered alternative schemes where the normal component was used, but they appeared less effective, possibly due to sideband pollutions of the feedback

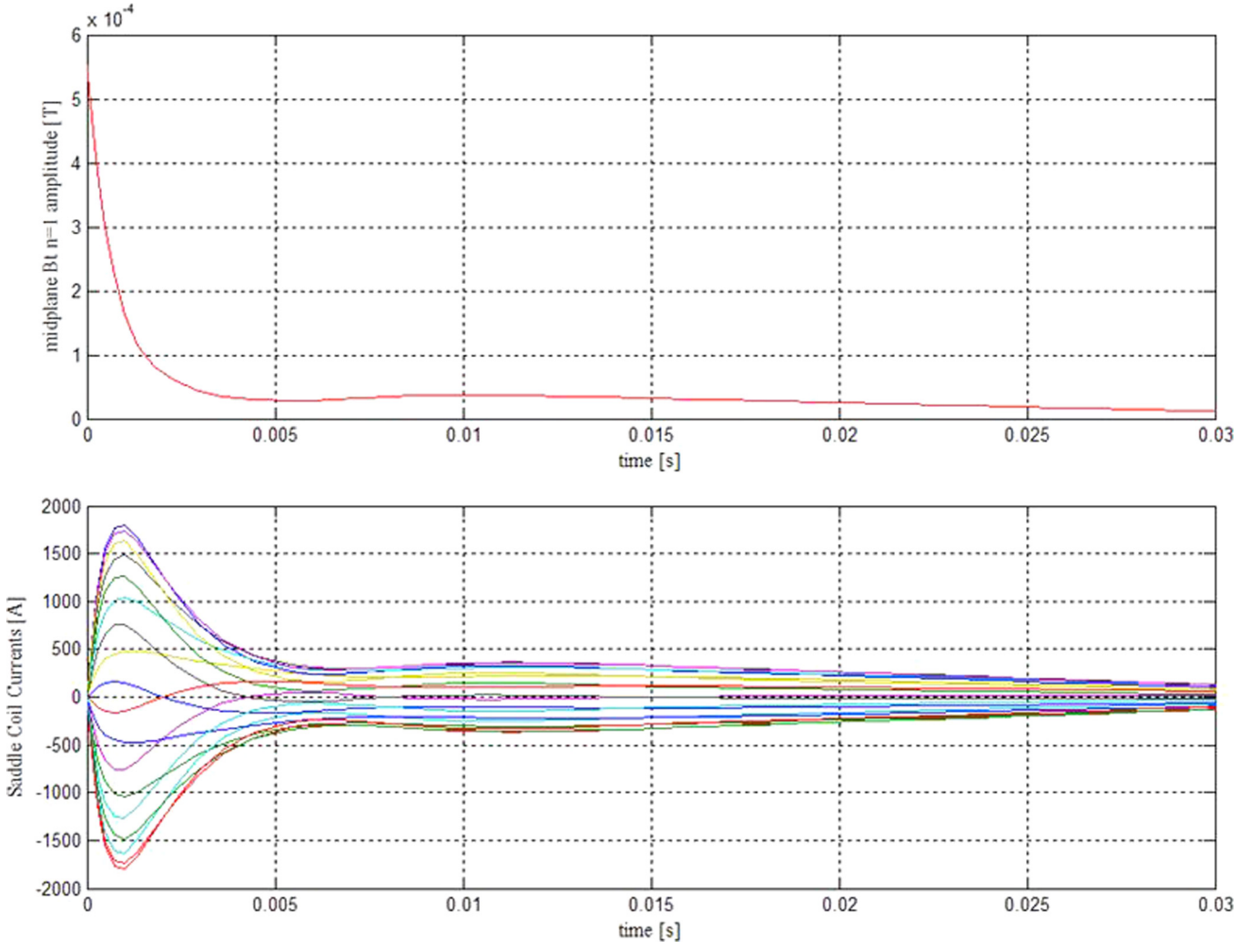

FIG. 15. Current-based proportional feedback controller: time evolution of midplane Bt $n = 1$ harmonic component and saddle coil currents.

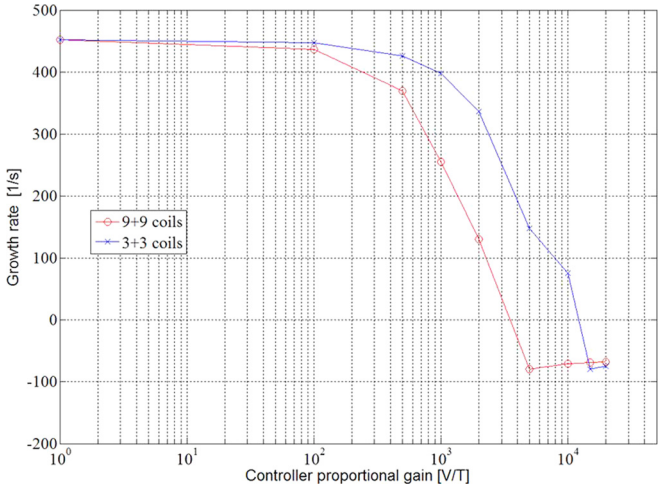

FIG. 16. Voltage-based feedback control. Growth rates of the eigenvector dominating the $n=1$ harmonic of the output signal: full (red circle) and reduced (blue crosses) set of coils are shown.

variable.[30] Thus, the $n=1$ harmonic component to be feedback was calculated taking the measurement of Bt at the equatorial plane of the machine. The inspection of the mode structure when no control is applied (i.e., in open loop), whose normal component is shown in Fig. 13, suggested to introduce a spatial phase shift of 180° between the control action of the upper and lower set of coils, equivalent to an anti-series connection.

A simple proportional controller was implemented to close the loop. In Fig. 14, we show the behaviour of the instability growth rate as a function of the proportional gain. Evidently, a critical value can be found, such that for gains above this threshold the mode is stabilized. The same procedure for the *a priori* determination of the critical gain has been validated experimentally on the RFX-mod device.[29]

Fig. 15 shows the time behaviour of the magnetic field and of the control coil currents, corresponding to a gain robustly providing stability. Evidently, the maximum current required for feedback stabilization of the mode is slightly above 2 kAT, well below the design limits.[8]

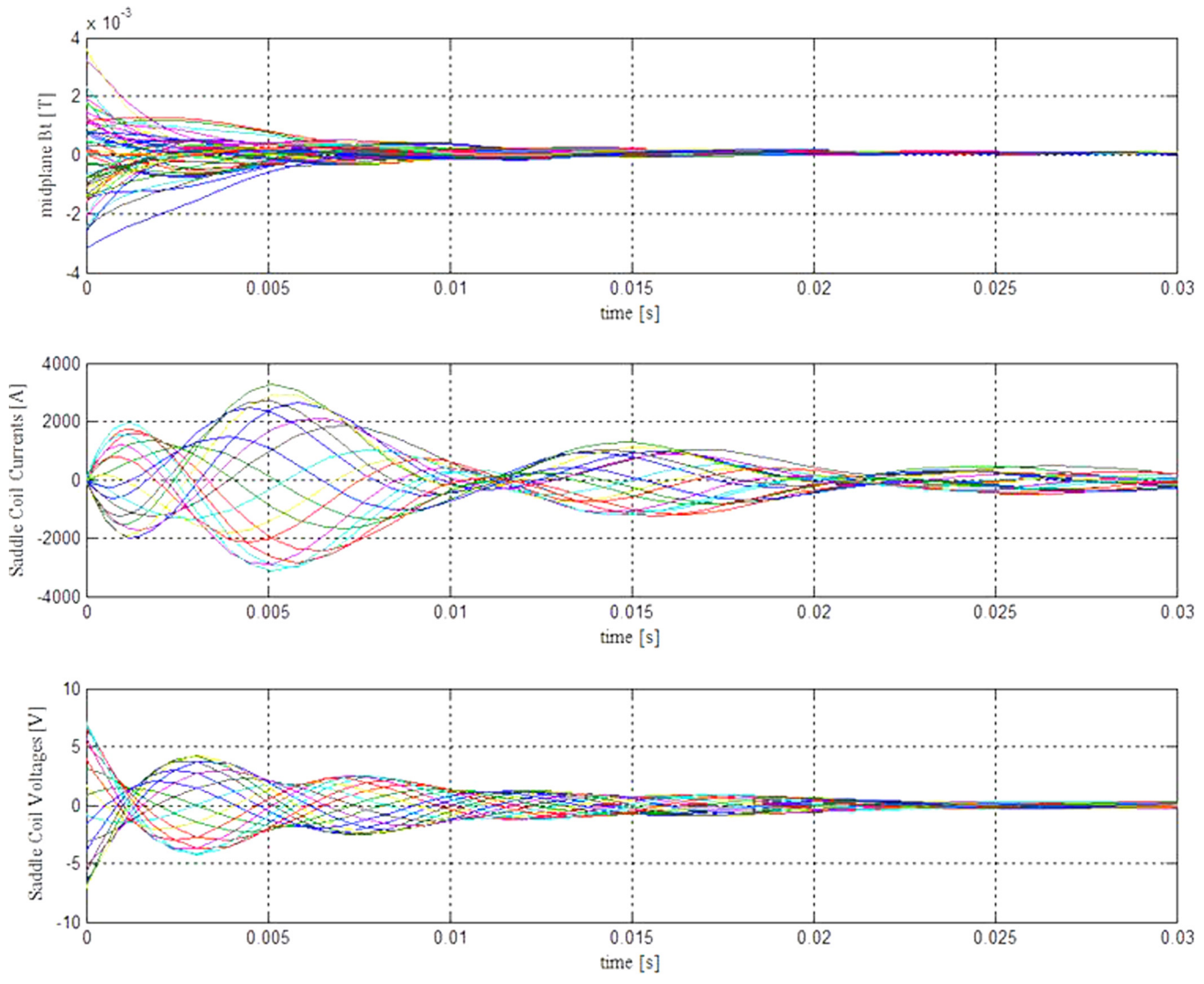

FIG. 17. Voltage-based proportional feedback controller: time evolution of Bt at midplane, saddle coil currents and voltages.

The stabilization of the mode can be accomplished even with a reduced set of control coils, although with a higher critical gain, as suggested in Ref. 31.

C. Voltage-based feedback control

Similar considerations have been repeated assuming that the feedback control acts directly on the $n=1$ voltage fed to the coils; evidently, this scheme does not require dedicated current regulators.

In Fig. 16, the growth rates associated to the eigenvectors with the largest $n=1$ harmonic content in the system output are shown as a function of the proportional gain for two sets of active coil. Due to the rigidity of the RWMs, the stabilization is achieved in the model even reducing the number of active coils to 3 in the upper set +3 in the lower set, instead of 9 + 9. The corresponding increase in the required gain is limited to 50%. Once the unstable mode has been suppressed, it can be still noticed the presence of modes, anyway stable, which exhibit an $n=1$ content in the output and are only marginally affected by the feedback action. In fact, their growth rates do not vary even when the gain is increased from 5000 to 20 000. As a consequence, the feedback signal extinguishes according to a time evolution dependent on the dynamic properties of these modes rather than on the control.

The time evolution of the Bt sensor measurements along with the coil currents and voltages are shown in Fig. 17, for a proportional gain $K_p = 10^3$. A random initial state has been chosen, giving rise to an initial amplitude of the $n=1$ harmonic of the magnetic field tangential component around 0.5 mT.

The relatively high values of the currents and low values of the voltages are consistent with the assumption of single turn, low resistance coils. This also explains the very slow decay of the coil currents when no voltage is applied by the control system. In any case, the power requirements are within the design values, suggesting that active stabilization

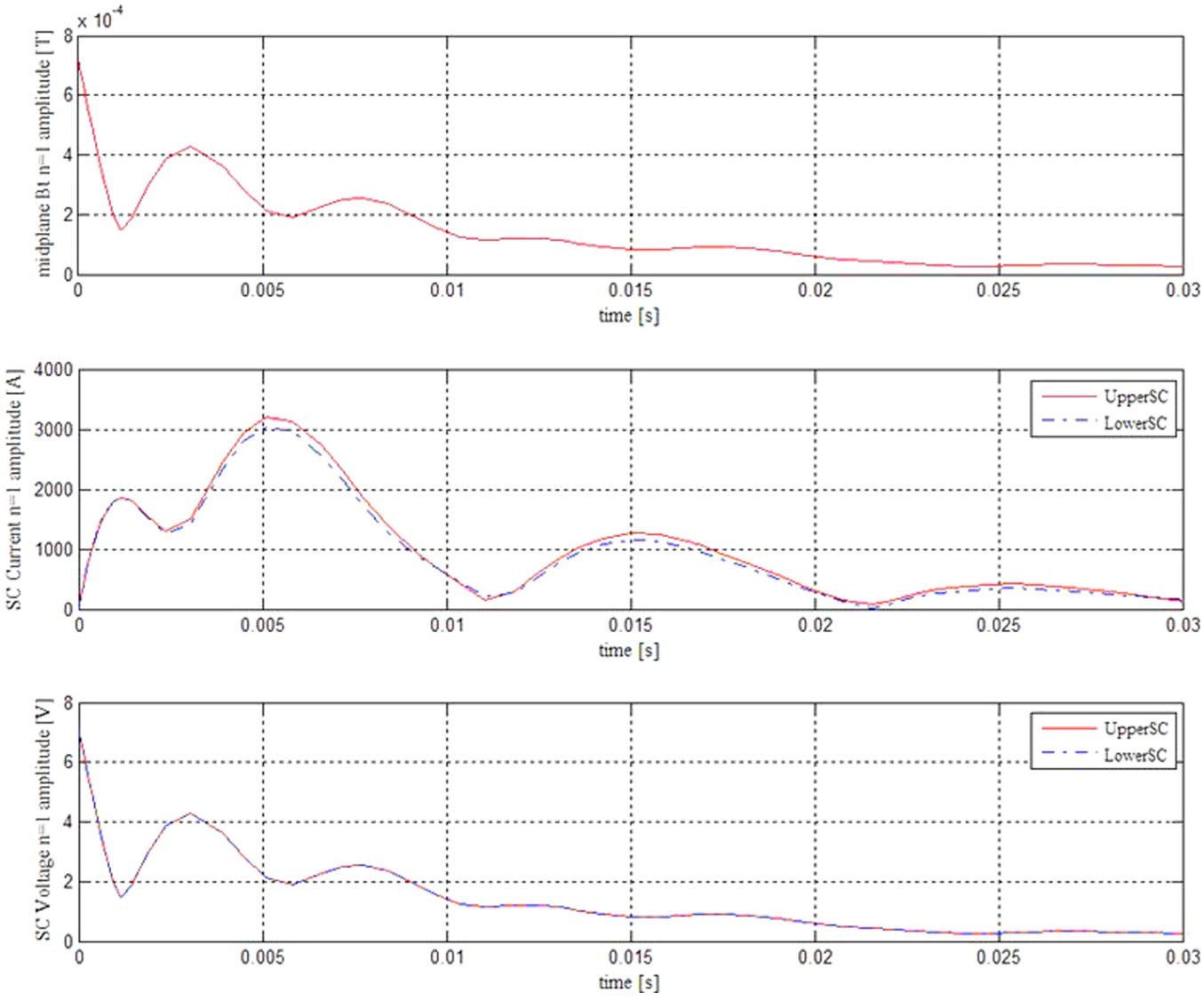

FIG. 18. Voltage-based proportional feedback controller: time evolution of $n=1$ harmonic component amplitude of midplane Bt, saddle coil currents and voltages.

of the $n=1$ RWM is indeed possible. In Fig. 18, the $n=1$ harmonic components are presented, too. In particular, while the requested voltages are perfectly symmetric, very small differences between upper and lower coil sets appear, possibly due to the asymmetry of the geometry and of the plasma response. The observed evolution of the $n=1$ component of Bt is in agreement with the expected dynamic content. It should be emphasized that the controller gain was chosen so as to assure stabilization of the system, but no attempt of optimizing the controller performances has been accomplished.

V. CONCLUSIONS AND PERSPECTIVE

Among the missions of the FAST proposal, one of the most important is to support ITER operations and to help in addressing the most worrying DEMO operational aspects. It is well recognized that in both cases the disruption problem is, by far, the most important one. A very rough classification of disruptions can be made by dividing them in events driven by energy balance collapse (i.e., radiative collapse) or by exceeding some machine limit (for instance low q_{95}, or high-β plasmas). Consequently, in order to attain a DEMO disruption-free operational regime, it will be necessary to study and implement different and integrated control systems and tools. For instance, recent experiments have shown the possibility to "control" the event of first type by an active feedback loop that uses Electron Cyclotron Heating to avoid the radiative collapse.[32,33] On the other side, so far, very few attempts have been done to experimentally test feedback loops capable to keep under control the onset of MHD modes when operating close to machine limits. Recently, the Reversed Field Pinch RFX (operated as a tokamak) has shown the possibility to avoid plasma disruptions connected to operations at $q_{95} \approx 2$.[10] In such experiments, and in other presently existing devices, it is only possible to show "the proof of principle." What is still missing is the proof that a suitable control system can be used to avoid the class of plasma disruptions associated with very low q_{95} regimes, when operating with magnetic and kinetic energy densities close to reactor values.

The present paper gives a contribution in this direction. To this purpose, a new FAST extreme scenario ($I_p = 10$MA, $q_{95} \sim 2.3$) has been designed, with different equilibrium pressure and current density profiles, corresponding to different conditions and MHD stability properties. A characterization of the ideal and resistive MHD modes (connected with $q_{95} \approx 2$) has been performed by including a fully 3D description of the real FAST structures, showing that in some cases a potentially dangerous MHD mode could explode.

Consequently, different types of closed loop feedback controllers (using current and/or voltage) have been investigated, showing the actual possibility to stabilize the dangerous $n=1$ RWM, by feeding with moderate currents and voltages the FAST internal coils. Such approach may not be necessarily imagined as an ultimate solution for a reactor, to allow operation at very high plasma current, hence improving the machine performances. Rather, it could be considered as a system that allows disruption avoidance, connected with operation at very low q_{95}. This could be obtained by slowing down the mode growth, hence giving the possibility to drive the plasma towards a safer operational space. Of course, the present paper is not intended to be exhaustive in showing the possibility to achieve disruption-free operational regimes in FAST and/or in any other machine. It simply gives a contribution towards the effective combination of various control tools for different classes of disruptions (see for instance[32,33]), with the final aim of attaining an actual disruption-free regime on DEMO.

Clearly, a number of open problems still remain: for instance, the effect of the $n=1$ tearing mode and the consequences of the fact that the $q=2$ surface is very close to the plasma edge. A positive role could be still played by the aforementioned ECCD control system; however, the lack of extensive experimental data about the use of ECCD in low-q scenarios makes it difficult to have a clear idea about the effectiveness of such a solution. In a close future, dedicated ECCD control experiments will be carried out on FTU, in order to get some indications and to give some preliminary answers to these points.

ACKNOWLEDGMENTS

This work was partly supported by Italian MIUR under PRIN Grant No. 2010SPS9B3.

[1]N. Hosogane, JT-60SA Design Team, Japan-Europe Satellite Tokamak Working Group, Fusion Sci. Technol. **52**, 375 (2007), see http://www.ans.org/pubs/journals/fst/a_1516.
[2]A. Pizzuto, F. Gnesotto, M. Lontano, R. Albanese, G. Ambrosino, M. L. Apicella, M. Baruzzo, A. Bruschi, G. Calabrò, A. Cardinali, R. Cesario, F. Crisanti, V. Cocilovo, A. Coletti, R. Coletti, P. Costa, S. Briguglio, P. Frosi, F. Crescenzi, V. Coccorese, A. Cucchiaro, C. Di Troia, B. Esposito, G. Fogaccia, E. Giovannozzi, G. Granucci, G. Maddaluno, R. Maggiora, M. Marinucci, D. Marocco, P. Martin, G. Mazzitelli, F. Mirizzi, S. Nowak, R. Paccagnella, L. Panaccione, G. L. Ravera, F. Orsitto, V. Pericoli Ridolfini, G. Ramogida, C. Rita, M. Santinelli, M. Schneider, A. A. Tuccillo, R. Zagórski, M. Valisa, R. Villari, G. Vlad, and F. Zonca, Nucl. Fusion **50**, 095005 (2010).
[3]M. Lontano and FAST Team, "FAST power exhaust in view of DEMO," in 27th SOFT Conference, Liege (2012), Paper No. OA5.4.
[4]F. Crisanti, A. Cucchiaro, R. Albanese, G. Artaserse, M. Baruzzo, T. Bolzonella, G. Brolatti, G. Calabrò, F. Crescenzi, R. Coletti, P. Costa, A. della Corte, A. Di Zenobio, P. Frosi, D. Harting, L. Lauro Taroni, G. Maddaluno, D. Marcuzzi, F. Maviglia, L. Muzzi *et al.*, Fusion Eng. Des. **86**, 497 (2011).
[5]V. Pericoli Ridolfini, R. Zagórski, G. Artaserse, G. Calabrò, F. Crisanti, G. Maddaluno, G. Ramogida, and B. Viola, J. Nucl. Mater. **438**, Supplement, S414–S417 (2013).
[6]I. Pagani, C. Bertolini, F. Crisanti, A. Cucchiaro, G. Di Gironimo, G. Ramogida, F. Crescenzi, and F. Lucca, "Preliminary electromagnetic design for divertor of FAST," in 27th SOFT Conference, Liege (2012) Paper No. P2.142.
[7]F. Romanelli, M. Laxåback, and on behalf of the JET EFDA Contributors, Nucl. Fusion **51**, 094008 (2011).
[8]G. Ramogida, G. Calabrò, V. Cocilovo, F. Crescenzi, F. Crisanti, A. Cucchiaro, G. Di Gironimo, R. Fresa, V. Fusco, P. Martin, S. Mastrostefano, R. Mozzillo, F. Nuzzolese, F. Renno, C. Rita, F. Villone, and G. Vlad, Fusion Eng. Des. **88**, 1156 (2013).
[9]J. Wesson, *Tokamaks* (Oxford University Press, 1997).
[10]M. Baruzzo, T. Bolzonella, R. Cavazzana, and Y. In, "Feedback control of the 2/1 mode in RFX-mod tokamak plasmas with qedge $\approx$ 2," in 38th EPS Conference, Strasbourg (2011), Paper No. P2.091.
[11]P. Piovesan *et al.*, "Tokamak operation with safety factor q 95 $<$ 2 via control of MHD stability," Phys. Rev. Lett. **113**, 045003 (2014).
[12]J. M. Hanson *et al.*, Phys. Plasmas **21**, 072107 (2014).
[13]G. Calabrò, F. Crisanti, G. Ramogida, P. Mantica, B. Baiocchi, A. Cucchiaro, P. Frosi, V. Fusco, Y. Liu, S. Mastrostefano, F. Villone, G. Vlad, and R. Fresa, Fusion Eng. Des. **88**, 858 (2013).

[14]G. Cenacchi and A. Taroni, "JETTO: A Free Boundary Plasma Transport Code (Basic Version)," Rapporto ENEA RT/TIB 1988 (5).
[15]R. E. Waltz, G. M. Staebler, W. Dorland, G. W. Hammett, M. Kotschenreuther, and J. A. Konings, Phys. Plasmas **4**, 2482 (1997).
[16]G. Calabrò, P. Mantica, B. Baiocchi, L. Lauro-Taroni, O. Asunta, M. Baruzzo, A. Cardinali, G. Corrigan, F. Crisanti, D. Farina, L. Figini, G. Giruzzi, F. Imbeaux, T. Johnson, M. Marinucci, V. Parail, A. Salmi, M. Schneider, and M. Valisa, in Fusion Energy 2010 (Proceedings of the 23rd International Conference, Daejeon, 2010), THC/P2-05, IAEA, Vienna.
[17]A. Bondeson, G. Vlad, and H. Lütjens. Phys. Fluids B **4**, 1889–1900 (1992).
[18]Y. Q. Liu, A. Bondeson, C. M. Fransson, B. Lennartson, and C. Breitholtz, Phys. Plasmas **7**, 3681 (2000).
[19]F. Villone, Y. Q. Liu, R. Paccagnella, T. Bolzonella, and G. Rubinacci, Phys. Rev. Lett. **100**, 255005 (2008).
[20]A. Portone, F. Villone, Y. Liu, R. Albanese, and G. Rubinacci, Plasma Phys. Controlled Fusion **50**, 085004 (2008).
[21]G. Calabrò, F. Crisanti, V. Fusco, Y. Liu, P. Martin, S. Mastrostefano, F. Villone, and G. Vlad, "MHD stability studies for high-current scenarios in FAST," in 39th EPS Conference, Stockholm (2012), Paper No. P2.079.
[22]M. Maraschek, Nucl. Fusion **52**, 074007 (2012).
[23]M. S. Chu and M. Okabayashi, Plasma Phys. Controlled Fusion **52**, 123001 (2010).
[24]A. M. Garofalo *et al.*, Nucl. Fusion **41**, 1171 (2001).
[25]E. J. Strait *et al.*, Phys. Plasmas **11**, 2505 (2004).
[26]S. A. Sabbagh, J.-W. Ahn, J. Allain, R. Andre, A. Balbaky, R. Bastasz, D. Battaglia, M. Bell, R. Bell, P. Beiersdorfer *et al.*, Nucl. Fusion **53**, 104007 (2013).
[27]F. Villone, Y. Liu, G. Rubinacci, and S. Ventre, Nucl. Fusion **50**, 125011 (2010).
[28]O. Katsuro-Hopkins, J. Bialek, D. A. Maurer, and G. A. Navratil, Nucl. Fusion **47**, 1157 (2007).
[29]G. Marchiori, M. Baruzzo, T. Bolzonella, Y. Q. Liu, A. Soppelsa, and F. Villone, Nucl. Fusion **52**, 023020 (2012).
[30]P. Zanca, L. Marrelli, R. Paccagnella, A. Soppelsa, M. Baruzzo, T. Bolzonella, G. Marchiori, P. Martin, and P. Piovesan, Plasma Phys. Controlled Fusion **54**, 094004 (2012).
[31]M. Baruzzo, T. Bolzonella, Y. Q. Liu, G. Manduchi, G. Marchiori, A. Soppelsa, M. Takechi, and F. Villone, Nucl. Fusion **52**, 103001 (2012).
[32]B. Esposito, G. Granucci, S. Nowak, J. R. Martin-Solis, L. Gabellieri, E. Lazzaro, P. Smeulders, M. Maraschek, G. Pautasso, J. Stober, W. Treutterer, L. Urso, F. Volpe, H. Zohm, FTU, ECRH, and ASDEX Upgrade Teams, Nucl. Fusion **49**, 065014 (2009).
[33] B. Esposito, G. Granucci, M. Maraschek, S. Nowak, E. Lazzaro, L. Giannone, A. Gude, V. Igochine, R. McDermott, E. Poli, M. Reich, F. Sommer, J. Stober, W. Suttrop, W. Treutterer, H. Zohm, ASDEX Upgrade, and FTU Teams, Plasma Phys. Controlled Fusion **53**, 124035 (2011).